Journal of Applied Polymer Science

Thermally and Magnetically Dual-Responsive Mesoporous Silica Nanospheres: Preparation, Characterization, and Properties for the Controlled Release of Sophoridine

Liling Dong,[1] Hailong Peng,[1,2] Shenqi Wang,[1] Zhong Zhang,[3] Jinhua Li,[3] Fanrong Ai,[4] Qiang Zhao,[1] Mei Luo,[1,2] Hua Xiong,[1] Lingxin Chen[3]

[1]State Key Laboratory of Food Science and Technology, Nanchang University, Nanchang 330047, China
[2]Department of Chemical Engineering, Nanchang University, Nanchang 330031, China
[3]Key Laboratory of Coastal Zone Environmental Processes and Ecological Remediation, Yantai Institute of Coastal Zone Research, Chinese Academy of Sciences, Yantai 264003, China
[4]Department of Mechanical Engineering, Nanchang University, Nanchang 330031, China
Correspondence to: H. Xiong (E-mail: huaxiong100@126.com) and L. Chen (E-mail: lxchen@yic.ac.cn)

ABSTRACT: Novel thermally and magnetically dual-responsive mesoporous silica nanoparticles [magnetic mesoporous silica nanospheres (M-MSNs)–poly(*N*-isopropyl acrylamide) (PNIPAAm)] were developed with magnetic iron oxide (Fe_3O_4) nanoparticles as the core, mesoporous silica nanoparticles as the sandwiched layer, and thermally responsive polymers (PNIPAAm) as the outer shell. M-MSN–PNIPAAm was initially used to control the release of sophoridine. The characteristics of M-MSN–PNIPAAm were investigated by transmission electron microscopy, Fourier transform infrared spectroscopy, X-ray diffraction, thermogravimetry, N_2 adsorption–desorption isotherms, and vibrating specimen magnetometry analyses. The results indicate that the Fe_3O_4 nanoparticles were incorporated into the M-MSNs, and PNIPAAm was grafted onto the surface of the M-MSNs via precipitation polymerization. The obtained M-MSN–PNIPAAm possessed superparamagnetic characteristics with a high surface area (292.44 m^2/g), large pore volume (0.246 mL/g), and large mesoporous pore size (2.18 nm). Sophoridine was used as a drug model to investigate the loading and release properties at different temperatures. The results demonstrate that the PNIPAAm layers on the surface of M-MSN–PNIPAAm effectively regulated the uptake and release of sophoridine. © 2014 Wiley Periodicals, Inc. J. Appl. Polym. Sci. **2014**, *131*, 40477.

KEYWORDS: biocompatibility; biomedical applications; functionalization of polymers; drug-delivery systems; stimuli-sensitive polymers

Received 7 December 2013; accepted 17 January 2014
DOI: 10.1002/app.40477

INTRODUCTION

Sophoridine is one of the main alkaloids extracted from *Sophora alopecuroides L*,[1] and it has a wide range of pharmacological properties, including various strong antitumor activities.[1,2] However, despite the attractive pharmacological properties of sophoridine, its therapeutic potential is significantly restricted by its wide distribution and rapid elimination *in vivo*.[3] To overcome these disadvantages, a number nanoparticle and microsphere delivery systems have been developed to encapsulate sophoridine.[4] Nevertheless, these organic carriers often suffer from various disadvantages, including instability in *in vivo* and *in vitro* environments, poor controlled release profiles, and common leakages of entrapped components in aqueous media.[4] Thus, the fabrication of novel inorganic-material-based nanocarriers for sophoridine encapsulation may be an effective approach for overcoming such challenges.

Considerable scientific attention has been paid to mesoporous silica nanoparticles (MSNs) because of their superior properties, such as their large surface areas, high pore volumes, tunable pore sizes, and easily modified outer surfaces.[5–8] MSNs possess good biocompatibility, low toxicity,[9,10] and excellent physical and chemical stability. MSNs have been widely applied in many fields, including sensors,[11–13] catalysis,[14,15] separation,[16] and drug delivery.[17–19] Numerous types of drugs and bioactive molecules of various sizes, shapes, and functionalities can be hosted in MSNs[20] because their poor channel sizes can be regulated. However, because loaded drugs burst when released from unmodified MSNs, various researchers have focused on exploring intelligent MSNs to overcome this advantage.[21]

Intelligent MSNs have been fabricated by the capping of the pores of MSNs with quantum dots, dendrimers, iron oxide, and gold nanoparticles to control drug uptake and release.[22,23]

However, this procedure is irreversible after cap removal, and nanovalve synthesis is a little complex; this limits the application of MSNs in drug-delivery systems. Reversible stimuli-responsive MSNs have recently been developed with pH-responsive,[24–26] thermally responsive,[27,28] and photoresponsive polymers.[29–31] The MSNs modified with such intelligent polymeric materials can control the uptake and release of guest molecules with external stimuli.

Poly(*N*-isopropyl acrylamide) (PNIPAAm) is a known intelligent polymer that is responsive to the temperature. PNIPAAm has the property of having a soluble (hydrophilic)–insoluble (hydrophobic) transition at a lower critical solution temperature (LCST) of about 32°C in water;[32,33] it exhibits a coil (soluble) state when the temperature is below the LCST and a collapsed (insoluble) state when the temperature is above the LCST.[34] Moreover, PNIPAAm is also among the smart polymers most commonly used to modify nanoparticles in drug-delivery systems.[35–37] The thermally responsive behavior of PNIPAAm can be used to design a smart nanoshell on the exterior surface of MSNs; this may be the ideal way to take up and control the release of drugs based on temperature changes.

The control of MSNs coated with PNIPAAm (MSN–PNIPAAm) on the uptake and release of drugs has been established. However, the delivery of drugs by MSN–PNIPAAm to a targeted site[38] is difficult and results in the decreased bioavailability of the drugs. Magnetic iron oxide (Fe_3O_4) nanomaterials have gained considerable attention because of their potential applications in medical fields and magnetically guided drug-delivery vehicles.[31,39–41] Hence, the integration of MSN–PNIPAAm with Fe_3O_4 could selectively deliver drugs to desired organs or tissues inside the body and thereby improve the bioavailability of drugs.

In this study, novel thermally and magnetically dual-responsive mesoporous silica nanoparticles [magnetic mesoporous silica nanospheres (M-MSNs)–PNIPAAm] were delicately prepared. To our knowledge, this successful application of M-MSN–PNIPAAm for the controlled uptake and release of sophoridine is the first such study in the field. The physicochemical characteristics of M-MSN–PNIPAAm were investigated systematically. The thermoresponsive behavior of PNIPAAm was used to design a smart nanoshell on the exterior surface of the M-MSNs, which could be reversibly switched between open and closed states with temperature changes. The M-MSN–PNIPAAm carrier proved potentially applicable for controlled and targeted drug delivery.

EXPERIMENTAL

Reagents and Materials

Hexadecyltrimethylammonium bromide (CTAB) and 3-(trimethoxysilyl)propyl methacrylate (MPS) were purchased from Sigma-Aldrich (Shanghai, China). Sophoridine (98%), purchased from Sinopharm Chemical Reagent Co., Ltd., was used with recrystallization from petroleum ether. Ferrous sulfate heptahydrate ($FeSO_4{\cdot}7H_2O$) and anhydrous iron(III) chloride ($FeCl_3$) were purchased from Sinopharm Chemical Reagent Co., Ltd. (Shanghai, China). *N*-Isopropyl acrylamide (NIPAAm), *N,N′*-methylene bisacrylamide (MBA), ammonium persulfate (APS), mesitylene, and tetraethyl orthosilicate (TEOS) were purchased from Aladdin Chemistry Co., Ltd. (Shanghai, China). The ammonia solution ($NH_3{\cdot}H_2O$; 25–28 wt %), ammonium nitrate (NH_4NO_3), anhydrous ethanol, and anhydrous toluene were purchased from Donghu Chemical Co., Ltd. (Nanchang, China).

Synthesis of Silica-Coated Fe_3O_4 (Fe_3O_4@SiO_2)

Superparamagnetic Fe_3O_4 nanoparticles were synthesized with the coprecipitation method.[39] The Fe_3O_4 nanoparticles (0.12 g) were dispersed in anhydrous ethanol (80 mL; $NH_3{\cdot}H_2O$, 5 mL). The solution was quickly added to an ethanol solution and maintained with stirring. The TEOS (1 mL) was added to the mixed solution in drops and was left to react for 12 h at room temperature. The Fe_3O_4@SiO_2 nanoparticles were separated by a permanent magnet and rinsed with anhydrous ethanol three times to remove the residual $NH_3{\cdot}H_2O$.

Modification of the M-MSNs with MPS

The Fe_3O_4@SiO_2 nanoparticles (90 mg) were dissolved in distilled water (160 mL) containing CTAB (1.0 g) and sonicated for 25 min. Afterward, mesitylene (2.5 mL) was added, and the mixture was stirred for 3 h. This was followed by the addition of $NH_3{\cdot}H_2O$ (16 mL) and TEOS (3 mL). The mixed system reacted for 6 h at 40°C. The M-MSN–CTAB product was collected by a magnet. M-MSN–CTAB (1.0 g) was dispersed in anhydrous toluene (100 mL), and this was followed by the addition of MPS (10 mL), which was reacted for 24 h at 50°C with nitrogen protection. The M-MSN–CTAB–MPS product was rinsed with anhydrous toluene to remove the unreacted MPS. The M-MSN–CTAB–MPS was placed into an NH_4NO_3 ethanol solution (200 mL, 10 mg/mL) to remove the CTAB and was refluxed for 6 h at 80°C. The product of M-MSN–MPS was dried *in vacuo*.

Preparation of M-MSN–PNIPAAm

The M-MSN–MPS was prepared through the seeded precipitation polymerization method. The detailed procedures are as follows. The monomers of NIPAAm (0.424 g) and MBA (22 mg) were dissolved in distilled water (200 mL). Subsequently, M-MSN–MPS (100 mg) was dispersed in the mixed solution by sonication for 20 min. An aqueous solution (5 mL) containing APS (13.4 mg) was added and heated to 70°C under nitrogen protection with stirring for 6 h. The M-MSN–PNIPAAm product was separated with a magnet, washed with distilled water, and dried *in vacuo* at 50°C.

Loading of M-MSN–PNIPAAm

M-MSN–PNIPAAm (25 mg) was dispersed into a sophoridine aqueous solution (20 mL, 0.1 mmol/L) with shaking for 24 h at 25 and 42°C, respectively. M-MSN–PNIPAAm was separated with a permanent magnet after sophoridine was loaded. The amount of free sophoridine in the supernatant (m_f) was measured by the high-performance liquid chromatography (HPLC) method. The loading efficiency could be calculated as follows:

$$\text{Loading efficiency } (\%) = \left(m_i - m_f\right)/m_i \times 100\%$$

where m_i is the initial amount of sophoridine.

Characterization

The amount of sophoridine was analyzed on a Shimadzu LC-10A system at 25°C with an HPLC pump operating at a flow

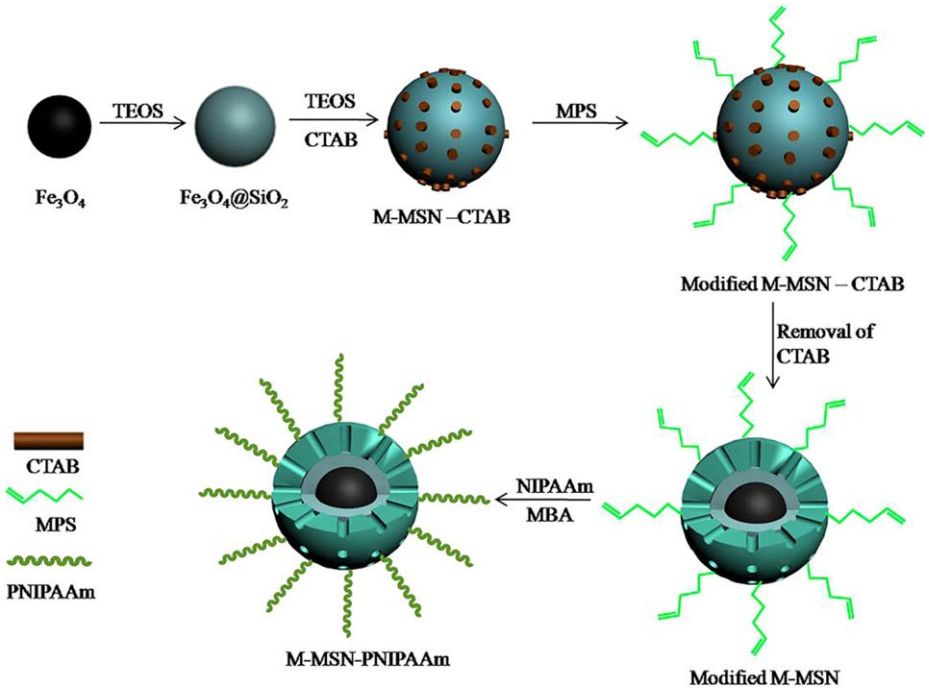

Scheme 1. Schematic for the preparation process of M-MSN–PNIPAAm. [Color figure can be viewed in the online issue, which is available at wileyonlinelibrary.com.]

rate of 1.0 mL/min. The analytical column was a 250 × 4.6 mm^2, 5-μm C_{18} column. The mobile phase was a acetonitrile/water/acetic acid (65:34:1 v/v/v) mixture. The detection wavelength was 250 nm for sophoridine.

The morphological characteristics of synthetic M-MSN–PNIPAAm were observed by transmission electron microscopy (TEM; JEM-2010HR, Japan). The X-ray diffraction (XRD) patterns of the samples were obtained from an X-ray diffractometer (XRD DI System, Bede, United Kingdom). The Fourier transform infrared (FTIR) spectra of the samples were obtained with a Nicolet 5700 FTIR system. Thermogravimetric analysis (TGA) was performed on a synchronous thermogravimetric analyzer (Thermogravimetric/Differential Thermal Analysis (TG/DTA) Pyris Diamond PE). The N_2 adsorption–desorption curves, specific surface area, total pore volume, and average pore size were measured with a fully automatic specific surface instrument (3H-2000PS1, Beishide Instruments, Beijing, China). Vibrating specimen magnetometry (VSM; 7407, Lakeshore) was used to examine the magnetic properties of the samples.

Release Kinetics of M-MSN–PNIPAAm

The sophoridine loaded M-MSN–PNIPAAm (10 mg) was immersed into phosphate buffer (10 mL, 0.01 mol/L, pH 7.4) and placed into water bath at 25 and 42°C with gentle stirring. At predetermined times, the supernatant (1 mL) was withdrawn and replaced with an equal volume of corresponding fresh media to maintain a constant volume. The amount of released sophoridine was determined by HPLC.

To determine the release mechanism of sophoridine from M-MSN–PNIPAAm, the release data were analyzed based on the zero-order, first-order, Higuchi, Hixson–Crowell, and Korsmeyer–Peppas models. The release exponent (n) of the Peppas model was also calculated with the Peppas method.[42,43] The model equations are as follows:

$$\text{Zero-order model}: Q_t/Q_\infty = kt$$

$$\text{First-order model}: \ln(1-Q_t/Q_\infty) = -kt$$

$$\text{Higuchi model}: Q_t/Q_\infty = kt^{1/2}$$

$$\text{Hixson–Crowell model}: (1-Q_t/Q_\infty)^{1/3} = -kt$$

$$\text{Korsmeyer–Peppas model}: \ln(Q_t/Q_\infty) = n\ln t + \ln k$$

where Q_t is the amount of sophoridine released in time t, Q_∞ is the total amount of sophoridine in M-MSN–PNIPAAm, k is an incorporating constant, and n is the release exponent indicating the release mechanism.

RESULTS AND DISCUSSION

Fabrication of M-MSN–PNIPAAm

The preparation process for M-MSN–PNIPAAm is illustrated in Scheme 1. Superparamagnetic Fe_3O_4 nanoparticles were synthesized with the coprecipitation method and were coated with a silica layer to improve the Fe_3O_4 stability. M-MSN–CTAB was then prepared with CTAB as a surfactant template and mesitylene as a pore-swelling agent. Subsequently, M-MSN–CTAB was modified by MPS, and vinyl groups were grafted onto the exterior surface of the M-MSNs. CTAB was removed through refluxing in NH_4NO_3–ethanol solutions to form the pores in the M-MSNs. Finally, the thermoresponsive material of PNIPAAm was grafted onto the surface of the M-MSNs by seeded precipitation polymerization with modified M-MSNs as seeds, APS as the initiator, MBA as the crosslinker, and NIPAAm as

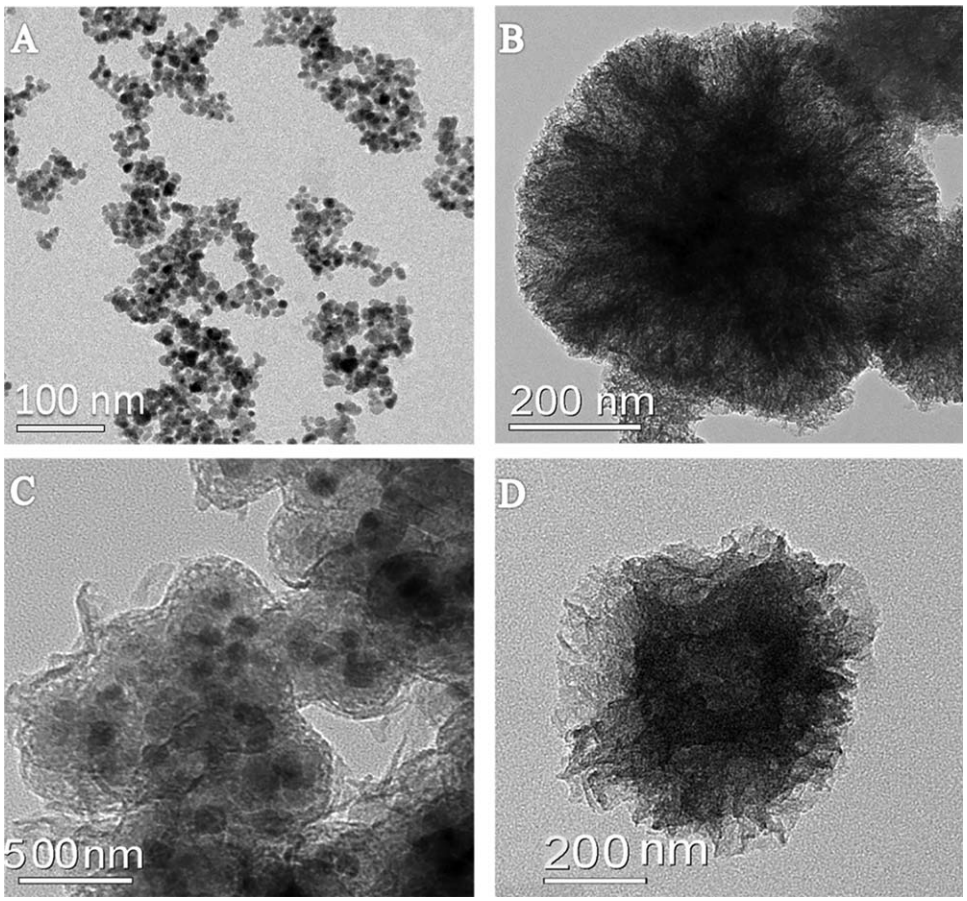

Figure 1. TEM images of (A) Fe_3O_4, (B) M-MSN, and (C, D) M-MSN–PNIPAAm.

the monomer. Consequently, the thermally responsive PNIPAAm material was formed on the surface of the M-MSNs.

Characterization of M-MSN–PNIPAAm

Information on the M-MSN–PNIPAAm structures was provided by TEM, and the results are shown in Figure 1. The M-MSNs were formed with Fe_3O_4 as the core and the MSNs as the shell [Figure 1(A,B)]. Regularly ordered pore channels were formed in the outer layer of the MSNs. However, the mesoporous pores of the M-MSNs disappeared with PNIPAAm coating on the surface of the M-MSNs [Figure 1(C,D)]. The results also indicate the serious aggregation phenomenon in M-MSN–PNIPAAm, which may have been due to the adhesion among PNIPAAm during the drying processes, and several M-MSNs were coated together by PNIPAAm during the polymerization processes.

The FTIR spectra of the samples are shown in Figure 2. The absorption band at 573 cm^{-1} was the stretching vibrations of Fe—O for Fe_3O_4. After the coating with silica layers, the adsorption peaks at 1081, 958, and 799 cm^{-1} were assigned to the Si—O—Si, Si—O—H, and Si—O groups, respectively; they demonstrated that the Fe_3O_4 nanoparticles were successfully coated by layers of silica. The absorption peaks at 2924 and 2854 cm^{-1} were due to the stretching of C—H from CTAB, which disappeared in the spectra of the M-MSNs. This suggested that CTAB was removed completely from M-MSN–CTAB. A new peak appeared at 1701 cm^{-1} in the spectrum of the M-MSN–MPS. This was the carbonyl group from MPS, and it demonstrated the successful grafting of the vinyl group onto the surface of the M-MSNs compared to the spectrum of the M-MSNs. The FTIR results of M-MSN–PNIPAAm showed that the absorption peaks at 1640 and 1539 cm^{-1} were the characteristic absorptions of the C—O (amide I) and N—H (amide II) groups from NIPAAm. The results suggest that the surface of the M-MSNs was successfully coated with PNIPAAm.

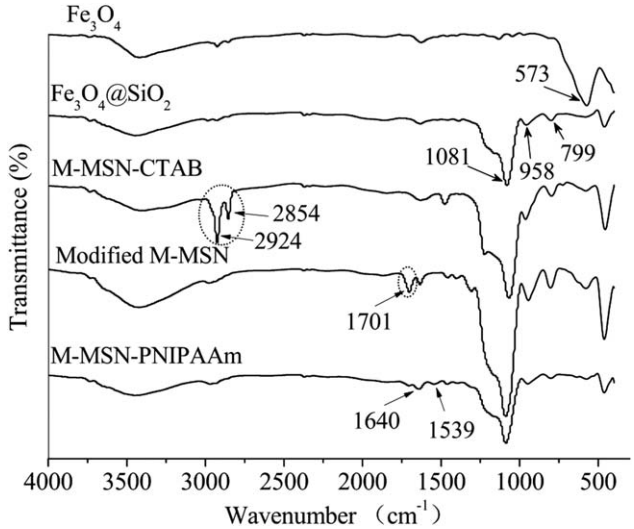

Figure 2. FTIR spectra of the Fe_3O_4, Fe_3O_4@SiO_2, M-MSN–CTAB, modified M-MSN, and M-MSN–PNIPAAm.

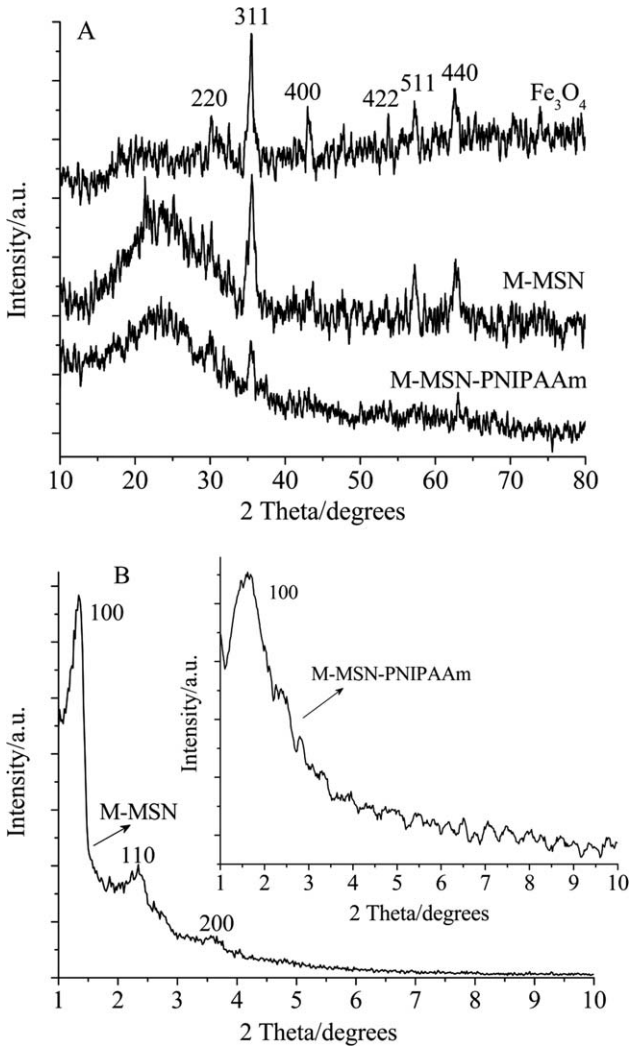

Figure 3. (A) Wide-angle XRD patterns of Fe_3O_4, M-MSN, and M-MSN–PNIPAAm and (B) small-angle XRD patterns of M-MSN and M-MSN–PNIPAAm.

The wide-angle XRD patterns are shown in Figure 3. The characteristic peaks of Fe_3O_4 ($2\theta = 30.12$, 35.41, 43.19, 53.67, 57.20, and 62.71°) were (220), (311), (400), (422), (511), and (440), respectively [Figure 3(A)]; this matched the Joint Committee on Powder Diffraction Standards (JSPDS) card number 19–629.[44,45] After the coating with the mesoporous silica layers, a new broad peak of silica appeared at around $2\theta = 23°$ for the M-MSNs. However, the intensity of the characteristic Fe_3O_4 peaks weakened after the grafting of PNIPAAm onto the outer surface of the M-MSNs. The ordered mesoporous structure of the M-MSNs was investigated by small-angle XRD, and the results are shown in Figure 3(B). A sharp peak appearing about at 1.35° was indexed as the (100) reflection; this indicated the ordered hexagonal mesoporous nanospheres existing on the outer layer of the M-MSNs. The (100) reflection remained with decreasing intensity after PNIPAAm modification; this demonstrated that the mesoporous structure was sustained after the coating with PNIPAAm on the surface of the M-MSNs.

The TGA curves of the M-MSNs and M-MSN–PNIPAAm are illustrated in Figure 4. The weight loss of M-MSNs at 11.70% may have been due to the disappearance of the MPS groups on the surface of the M-MSNs. The weight loss of M-MSN–PNIPAAm at approximately 39.52% due to PNIPAAm decomposition indicated that PNIPAAm was successfully grafted onto the surface of the M-MSNs.

The N_2 adsorption–desorption isotherms and M-MSNs and M-MSN–PNIPAAm pore size distributions are shown in Figure 5. The isotherms for M-MSNs and M-MSN–PNIPAAm were typical type IV curves; this confirmed that homogeneous mesoporous pore structures existed in the M-MSNs and M-MSN–PNIPAAm. The Brunauer–Emmett–Teller surface area and M-MSN total volumes were 442.22 m^2/g and 0.352 mL/g, respectively. After PNIPAAm grafting, the Brunauer–Emmett–Teller surface area (292.44 m^2/g) and M-MSN total volume (0.246 mL/g) were significantly decreased. The sharp peaks shown in Figure 5 indicate the mesoporous pore size distributions of the M-MSNs and M-MSN–PNIPAAm. The average mesoporous pore sizes of the M-MSNs and M-MSN–PNIPAAm were 4.32 and 2.18 nm, respectively [Figure 5(B)]. These results confirm that PNIPAAm was grafted onto the surface of the M-MSNs, whereas a few mesoporous pores were occupied by PNIPAAm.

The magnetic properties of Fe_3O_4 and M-MSN–PNIPAAm were observed by VSM, and the magnetic hysteresis loops are shown in Figure 6. The remanence or coercivity almost disappeared; this indicated the superparamagnetic characteristics of the Fe_3O_4 and M-MSN–PNIPAAm [Figure 6(A,B)]. The saturation magnetization values of Fe_3O_4 and M-MSN–PNIPAAm were 66.45 and 2.14 emu/g, respectively, and the separation time by the magnet were 5 and 60 s accordingly [Figure 6(C,D)]. The magnetization readings divided by the polymers of PNIPAAm resulted in the saturation magnetization and a decrease in the separation time for M-MSN–PNIPAAm.[39,46] M-MSN–PNIPAAm was proven to be highly sensitive to the magnetic field, and thus, it could serve as a targeting drug-delivery carrier with an external magnetic field.

Loading Efficiency of Sophoridine in M-MSN–PNIPAAm

Sophoridine was used as a model molecule to investigate the loading efficiency of M-MSN–PNIPAAm. The loading

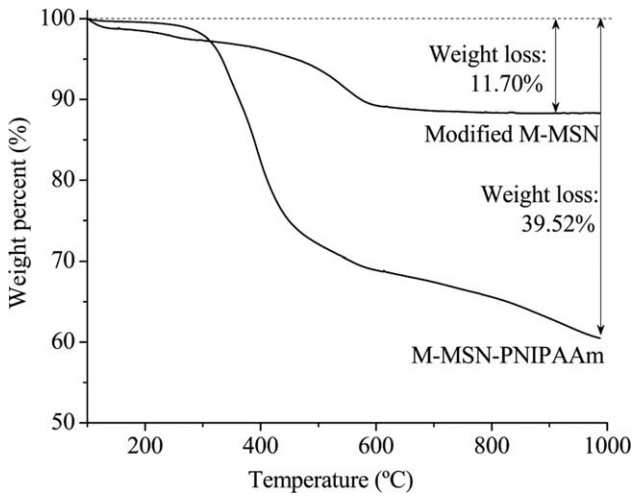

Figure 4. TGA curves of the modified M-MSN and M-MSN–PNIPAAm.

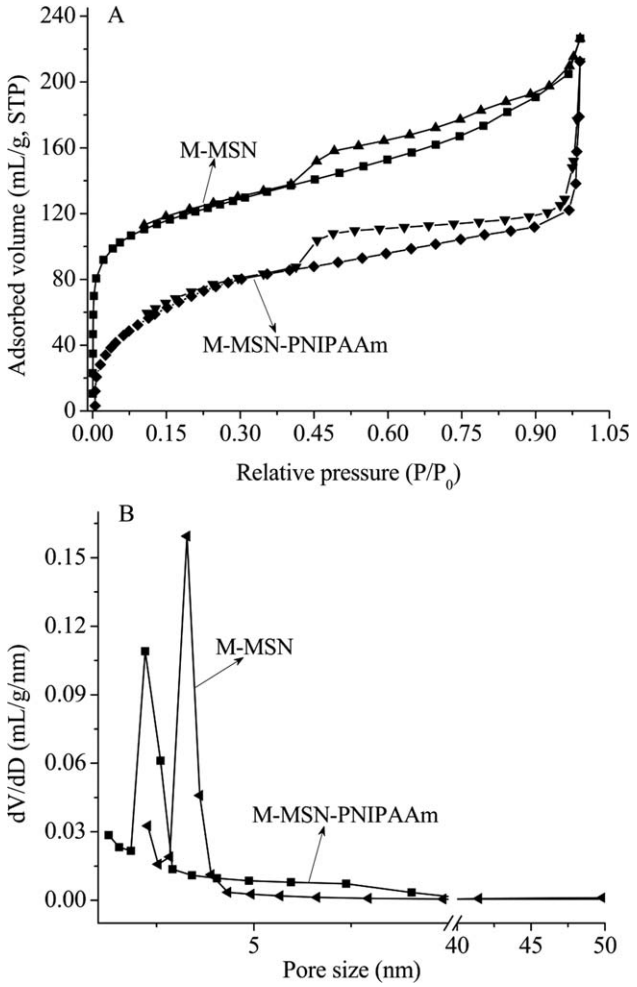

Figure 5. (A) N_2 adsorption–desorption isotherms and (B) mesoporous pore distribution of M-MSN and M-MSN–PNIPAAm. Here, "P" means "transient pressure", "P_0" means "initial pressure", and "P/P_0" means "nitrogen partial pressure"; "dV/dD" means "differential calculus of cumulative pore volume and average pore diameter".

efficiencies were about 46.54 and 18.69% at 25 and 42°C, respectively, for M-MSN–PNIPAAm. The solubility of the PNIPAAm chains in water gradually decreased in quality with increasing temperature. The long PNIPAAm chains collapsed toward the surface of M-MSN–PNIPAAm;[47] this blocked the pore entrance and lowered the loading efficiency at 42°C for M-MSN–PNIPAAm.

In Vitro Release and Release Kinetics of M-MSN–PNIPAAm

The *in vitro* release experiments were carried out at 25°C (below the LCST) and 42°C (above the LCST), respectively.[27,34] The *in vitro* release results of sophoridine from M-MSN–PNIPAAm are shown in Figure 7. The results indicate two stages of sophoridine release from M-MSN–PNIPAAm. The first stage of release was initially rapid, which may have been due to the rapid diffusion of the sophoridine on the surface of M-MSN–PNIPAAm. The second stage of release from M-MSN–PNIPAAm was slower in comparison. The amount of sophoridine released from M-MSN–PNIPAAm was about 25.01% for the first 10 h at 25°C. Subsequently, the release rate gradually slowed down, and the cumulative release amount reached approximately 64.45% at 50 h. However, the release rate was significantly lower at 42°C, and the cumulative release amount of sophoridine from M-MSN–PNIPAAm was only about 25.95% at 50 h. As established, PNIPAAm was sensitive to temperature, with an LCST at about 32°C.[39] Once the solution temperature of M-MSN–PNIPAAm was lower than the LCST, the outer layer of the PNIPAAm chains absorbed water, and the solubility state appeared. The soluble PNIPAAm chains resulted in the opening of pore entrances at 25°C. The release of sophoridine from M-MSN–PNIPAAm into solutions then became easy. Meanwhile, at 42°C (above the LCST), the PNIPAAM chains shrunk and collapsed toward the surface of the M-MSN–PNIPAAm.[48] Consequently, the pore entrances were blocked, and these significantly obstructed the release amount of sophoridine from the voids of M-MSN–PNIPAAm. Therefore, the release behavior of M-MSN–PNIPAAm could be regulated by changes in the external temperature, which controlled the release of drugs.

To evaluate the release mechanism of sophoridine from M-MSN–PNIPAAm, the zero-order, first-order, Higuchi, Hixson–Crowell, and Peppas models were used to match the release behaviors. The results of the correlation coefficient (R^2) are shown in Table I. The value of R^2 of the Higuchi model was higher than those of the other models at 42°C; this demonstrated that the Higuchi model was the most suitable model for

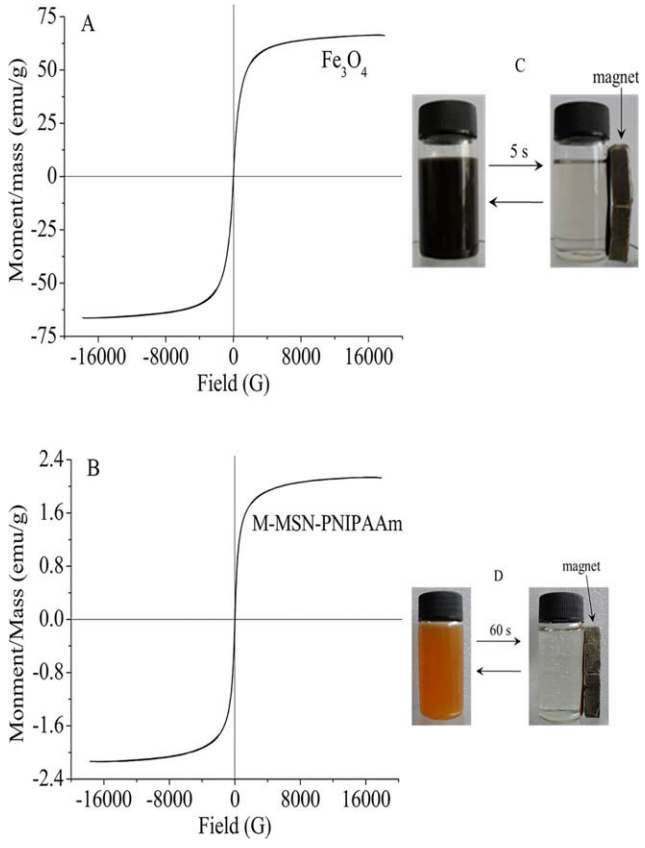

Figure 6. VSM curves of (A) Fe_3O_4 and (B) M-MSN–PNIPAAm. [Color figure can be viewed in the online issue, which is available at wileyonlinelibrary.com.]

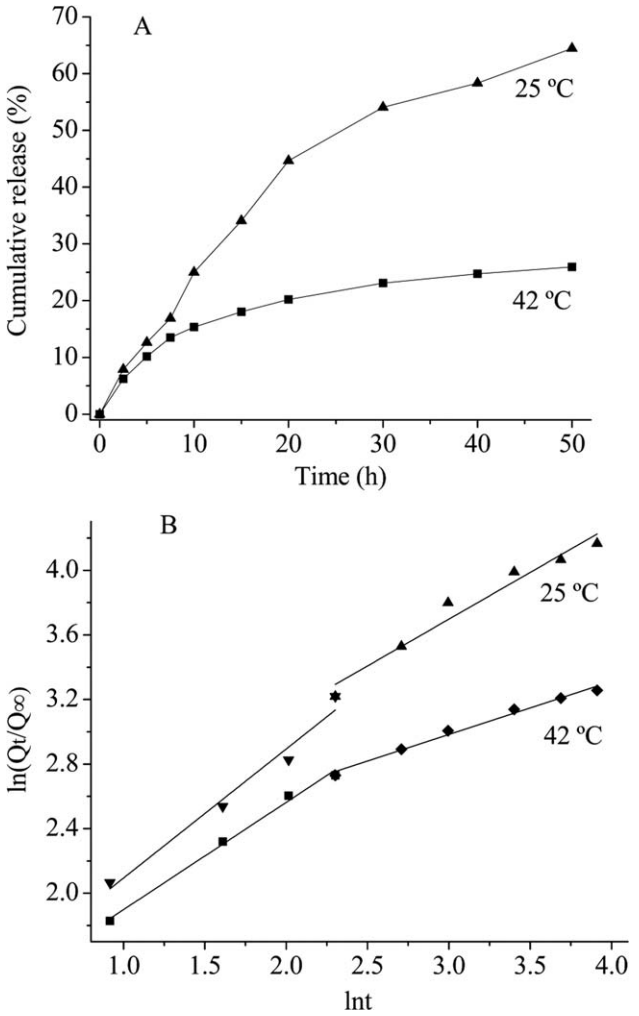

Figure 7. (A) Cumulative release curves and (B) Korsmeyer–Peppas kinetics of sophoridine from M-MSN–PNIPAAm at 25 and 42°C.

describing the sophoridine release kinetics from M-MSN–PNIPAAm at high temperatures. The results likewise indicate that the zero-order and Higuchi models demonstrated the release mechanism of sophoridine from M-MSN–PNIPAAm at 25°C for the first and second stages, respectively. The value of n indicates the release mechanism of the Peppas model, for example, $n = 0.43$ for typical Fickian diffusion, $n = 0.85$ for erosion transport, and $0.43 < n < 0.85$ for nontypical Fickian transport.[49] The n values of M-MSN–PNIPAAm were 0.665 and 0.799 for the rapid stages at 25 and 42°C, respectively. The results indicate that nontypical Fickian diffusion was the main release mechanism for M-MSN–PNIPAAm in the first stage. The n values of M-MSN–PNIPAAm were 0.579 and 0.328 for the second stage at 25 and 42°C, respectively. This showed that nontypical Fickian diffusion was the main release mechanism at 25°C, whereas typical Fickian diffusion was the main release mechanism at 42°C in this stage.

Table I. R^2 and n Values

	42°C		25°C	
Model	0–10 h	10–50 h	0–10 h	10–50 h
Zero-order R^2	0.963	0.919	0.964	0.901
First-order R^2	0.968	0.930	0.949	0.956
Higuchi R^2	0.992	0.971	0.915	0.957
Hixson-Crowell R^2	0.967	0.926	0.955	0.940
Korsmeyer–Peppas				
R^2	0.992	0.985	0.965	0.953
n	0.665	0.328	0.799	0.579

CONCLUSIONS

A novel thermally and magnetically dual-responsive nanocarrier (M-MSN–PNIPAAm) for loading sophoridine was successfully prepared by the incorporation of magnetic nanoparticles, mesoporous silica, and thermally responsive polymers. The PNIPAAm layer on the surface of the MSNs could be reversibly opened and closed as triggered by various temperatures and, thus, could regulate the uptake and release of sophoridine from M-MSN–PNIPAAm. M-MSN–PNIPAAm possessed superparamagnetic properties and could be guided to the target site by external magnetic fields. Therefore, M-MSN–PNIPAAm possesses thermally and magnetically dual-responsive functions for the controlled and targeted release of drugs and shows great application potential for drug-delivery systems.

ACKNOWLEDGMENTS

This work was funded by the National Natural Science Foundation of China (contract grant numbers 21201098, 51102131, 31160317, 21275158, and 21105117), the Jiangxi Department of Education Fund (contract grant number GJJ13039), and the Specialized Research Fund for the Doctoral Program of Higher Education (contract grant number 20113601110004).

AUTHOR CONTRIBUTION

Liling Dong and Hailong Peng contributed equally to this article. In this study, Liling Dong organized the data and wrote the manuscript. Hailong Peng performed the loading and release experiments and the high-performance liquid chromatography analysis. Shenqi Wang synthesized mesoporous silica nanospheres–poly(*N*-isopropyl acrylamide). Zhong Zhang and Jinhua Li revised the manuscript. Fanrong Ai provided the optimal conditions for the preparation of iron oxide. Qiang Zhao and Mei Luo submitted suggestions for improving the manuscript. Hua Xiong supervised the research and contacted the analysis and testing center of Nanchang University to provide the characterization analysis. Lingxin Chen supervised the research and contributed to the manuscript.

REFERENCES

1. Liang, L.; Wang, X. Y.; Zhang, X. H.; Ji, B.; Yan, H. C.; Deng, H. Z.; Wu, X. R. *Life Sci.* **2012**, *91*, 1295.
2. Wang, H.; Guo, S.; Qian, D.; Qian, Y.; Duan, J. A. *J. Pharm. Biomed. Anal.* **2012**, *67*, 16.
3. Zhang, Y.; Zhu, H.; Ye, G.; Huang, C.; Yang, Y.; Chen, R.; Yu, Y.; Cui, X. *Life Sci.* **2006**, 78, 1998.

4. Peng, H.; Dong, R.; Wang, S.; Zhang, Z.; Luo, M.; Bai, C.; Zhao, Q.; Li, J.; Chen, L.; Xiong, H. *Int. J. Pharm.* **2013**, *446*, 153.
5. Slowing, I. I.; Vivero-Escoto, J. L.; Wu, C. W.; Lin, V. S. *Adv. Drug Delivery Rev.* **2008**, *60*, 1278.
6. Hernandez, R.; Tseng, H.-R.; Wong, J. W.; Stoddart, J. F.; Zink, J. I. *J. Am. Chem. Soc.* **2004**, *126*, 3370.
7. Xu, S.; Li, J.; Chen, L. *J. Mater. Chem.* **2011**, *21*, 4346.
8. Slowing, I. I.; Trewyn, B. G.; Lin, V. S. Y. *J. Am. Chem. Soc.* **2007**, *129*, 8845.
9. Climent, E.; Martinez-Manez, R.; Sancenon, F.; Marcos, M. D.; Soto, J.; Maquieira, A.; Amoros, P. *Angew. Chem. Int. Ed. Engl.* **2010**, *49*, 7281.
10. Lu, J.; Liong, M.; Li, Z.; Zink, J. I.; Tamanoi, F. *Small* **2010**, *6*, 1794.
11. Yamada, T.; Zhou, H. S.; Uchida, H.; Tomita, M.; Ueno, Y.; Honma, I.; Asai, K.; Katsube, T. *Micropor. Mesopor. Mater.* **2002**, *54*, 269.
12. Wang, G.; Chen, Z.; Wang, W.; Yan, B.; Chen, L. *Analyst* **2011**, *136*, 174.
13. Wang, G.; Chen, Z.; Chen, L. *Nanoscale* **2011**, *3*, 1756.
14. Handa, P.; Holmberg, K.; Sauthier, M.; Castanet, Y.; Mortreux, A. *Micropor. Mesopor. Mater.* **2008**, *116*, 424.
15. Pandya, P. H.; Jasra, R. V.; Newalkar, B. L.; Bhatt, P. N. *Micropor. Mesopor. Mater.* **2005**, *77*, 67.
16. Son, W.-J.; Choi, J.-S.; Ahn, W.-S. *Micropor. Mesopor. Mater.* **2008**, *113*, 31.
17. Zhu, Y.; Fang, Y.; Borchardt, L.; Kaskel, S. *Micropor. Mesopor. Mater.* **2011**, *141*, 199.
18. Thomas, M. J. K.; Slipper, I.; Walunj, A.; Jain, A.; Favretto, M. E.; Kallinteri, P.; Douroumis, D. *Int. J. Pharm.* **2010**, *387*, 272.
19. Carino, I. S.; Pasqua, L.; Testa, F.; Aiello, R.; Puoci, F.; Iemma, F.; Picci, N. *Drug Delivery* **2007**, *14*, 491.
20. Zhang, J.; Li, X.; Rosenholm, J. M.; Gu, H. C. *J. Colloid Interface Sci.* **2011**, *361*, 16.
21. Nguyen, T. D.; Liu, Y.; Saha, S.; Leung, K. C. F.; Stoddart, J. F.; Zink, J. I. *J. Am. Chem. Soc.* **2007**, *129*, 626.
22. Lai, C.-Y.; Trewyn, B. G.; Jeftinija, D. M.; Jeftinija, K.; Xu, S.; Jeftinija, S.; Lin, V. S. Y. *J. Am. Chem. Soc.* **2003**, *125*, 4451.
23. Giri, S.; Trewyn, B. G.; Stellmaker, M. P.; Lin, V. S. *Angew. Chem. Int. Ed. Engl.* **2005**, *44*, 5038.
24. Hong, C.-Y.; Li, X.; Pan, C.-Y. *J. Mater. Chem.* **2009**, *19*, 5155.
25. Wu, H.; Tang, L.; An, L.; Wang, X.; Zhang, H.; Shi, J.; Yang, S. *React. Funct. Polym.* **2012**, *72*, 329.
26. Leung, K. C. F.; Nguyen, T. D.; Stoddart, J. F.; Zink, J. I. *Chem. Mater.* **2006**, *18*, 5919.
27. Zhu, Y.; Kaskel, S.; Ikoma, T.; Hanagata, N. *Micropor. Mesopor. Mater.* **2009**, *123*, 107.
28. Liu, C.; Guo, J.; Yang, W.; Hu, J.; Wang, C.; Fu, S. *J. Mater. Chem.* **2009**, *19*, 4764.
29. Zhu, Y.; Shi, J.; Shen, W.; Dong, X.; Feng, J.; Ruan, M.; Li, Y. *Angew. Chem. Int. Ed. Engl.* **2005**, *44*, 5083.
30. Cai, W.; Gupta, R. B. *J. Appl. Polym. Sci.* **2002**, *83*, 169.
31. Xu, S.; Li, J.; Song, X.; Liu, J.; Lu, H.; Chen, L. *Anal. Methods* **2013**, *5*, 124.
32. Rahman, M. M.; Chehimi, M. M.; Fessi, H.; Elaissari, A. *J. Colloid Interface Sci.* **2011**, *360*, 556.
33. Wakamatsu, H.; Yamamoto, K.; Nakao, A.; Aoyagi, T. *J. Magn. Magn. Mater.* **2006**, *302*, 327.
34. You, Y.-Z.; Kalebaila, K. K.; Brock, S. L.; Oupický, D. *Chem. Mater.* **2008**, *20*, 3354.
35. Kopeček, J. *Eur. J. Pharm. Sci.* **2003**, *20*, 1.
36. Eeckman, F.; Moes, A. J.; Amighi, K. *Int. J. Pharm.* **2004**, *273*, 109.
37. Fang, J. Y.; Chen, J. P.; Leu, Y. L.; Hu, J. W. *Drug Delivery* **2008**, *15*, 235.
38. Fu, Q.; Rama Rao, G. V.; Ward, T. L.; Lu, Y.; Lopez, G. P. *Langmuir* **2006**, *23*, 170.
39. Yao, A.; Chen, Q.; Ai, F.; Wang, D.; Huang, W. *J. Mater. Sci. Mater. Med.* **2011**, *22*, 2239.
40. Zhang, X. Y.; Chen, F. H.; Ni, J. Z. *Drug Delivery* **2009**, *16*, 280.
41. Xu, S.; Lu, H.; Zheng, X.; Chen, L. *J. Mater. Chem. C* **2013**, *1*, 4406.
42. Yan, S.; Zhu, J.; Wang, Z.; Yin, J.; Zheng, Y.; Chen, X. *Eur. J. Pharm. Biopharm.* **2011**, *78*, 336.
43. Peng, H.; Xiong, H.; Li, J.; Xie, M.; Liu, Y.; Bai, C.; Chen, L. *Food Chem.* **2010**, *121*, 23.
44. Lu, F.; Li, H.; Sun, M.; Fan, L.; Qiu, H.; Li, X.; Luo, C. *Anal. Chim. Acta* **2012**, *718*, 84.
45. Kong, X.; Gao, R.; He, X.; Chen, L.; Zhang, Y. *J. Chromatogr. A* **2012**, *1245*, 8.
46. Vestal, C. R.; Zhang, Z. *J. Nano. Lett.* **2003**, *3*, 1739.
47. Wang, X.; Liu, P.; Tian, Y. *J. Solid State Chem.* **2011**, *184*, 1571.
48. Hong, C.-Y.; Li, X.; Pan, C.-Y. *J. Phys. Chem. C* **2008**, *112*, 15320.
49. Ritger, P. L.; Peppas, N. A. *J. Controlled Release* **1987**, *5*, 37.